Journal of Power Sources 185 (2008) 6–12

Contents lists available at ScienceDirect

Journal of Power Sources

journal homepage: www.elsevier.com/locate/jpowsour

Platinum nanoparticles embedded in layer-by-layer films from SnO_2/polyallylamine for ethanol electrooxidation

Caroline B. Barretto[a], Renato L.T. Parreira[a], Rogéria R. Gonçalves[a], Dayse C. de Azevedo[b], Fritz Huguenin[a,*]

[a] Departamento de Química, Faculdade de Filosofia, Ciências e Letras de Ribeirão Preto, Universidade de São Paulo, 14040-901 Ribeirão Preto SP, Brazil
[b] NovoCell Energy Systems S.A., 13478-722 Americana SP, Brazil

ARTICLE INFO

Article history:
Received 19 June 2008
Received in revised form 11 July 2008
Accepted 15 July 2008
Available online 23 July 2008

Keywords:
Ethanol electrooxidation
Self-assembled film
Layer-by-layer
SnO_2
Polyallylamine
Platinum nanoparticle

ABSTRACT

Self-assembled films from SnO_2 and polyallylamine (PAH) were deposited on gold via ionic attraction by the layer-by-layer (LbL) method. The modified electrodes were immersed into a H_2PtCl_6 solution, a current of 100 μA was applied, and different electrodeposition times were used. The SnO_2/PAH layers served as templates to yield metallic platinum with different particle sizes. The scanning tunnel microscopy images show that the particle size increases as a function of electrodeposition time. The potentiodynamic profile of the electrodes changes as a function of the electrodeposition time in 0.5 mol L^{-1} H_2SO_4, at a sweeping rate of 50 mV s^{-1}. Oxygen-like species are formed at less positive potentials for the Pt–SnO_2/PAH film in the case of the smallest platinum particles. Electrochemical impedance spectroscopy measurements in acid medium at 0.7 V show that the charge transfer resistance normalized by the exposed platinum area is 750 times greater for platinum electrode (300 kΩ cm^2) compared with the Pt–SnO_2/PAH film with 1 min of electrodeposition (0.4 kΩ cm^2). According to the Langmuir–Hinshelwood bifunctional mechanism, the high degree of coverage with oxygen-like species on the platinum nanoparticles is responsible for the electrocatalytic activity of the Pt–SnO_2/PAH concerning ethanol electrooxidation. With these features, this Pt–SnO_2/PAH film may be grown on a proton exchange membrane (PEM) in direct ethanol fuel cells (DEFC).

1. Introduction

Among the various types of proton exchange membrane (PEM) fuel cells (PEMFCs), direct ethanol fuel cells (DEFCs) are especially promising for several power applications ranging from portable and stationary power supplies to transportation [1]. Ethanol has a higher theoretical mass energy (8 kW h Kg^{-1}) than other alcohols, such as methanol (6.1 kW h Kg^{-1}) [2], which has also been much studied [3]. Micro-fuel cells based on DEFCs are the best alternatives to compete with the lithium ion secondary batteries as an energy supply for the new generation of portable electronic devices. Contrary to secondary batteries, DEFCs can provide continuous power as long as ethanol is provided. Moreover, ethanol presents low toxicity and is a renewable biofuel obtained in large amounts from biomass fermentation.

Complete ethanol electrooxidation involves 12 electrons per alcohol molecule. Moreover, cleavage of the C–C bond is necessary for oxidation of ethanol to carbon dioxide. Because ethanol electrooxidation is more complicated than the oxidation of other substances employed as fuel, more active and selective electrocatalysts have been produced and studied. Platinum alloys have proven to be the best catalysts for ethanol oxidation and may be used as anodes in DEFCs [4–6]. A conclusion from such studies is that the use of platinum is mandatory, so DEFC commercialization is hampered by the high cost of the platinum catalyst. This has motivated the investigation into the electrocatalysis of novel materials, so as to obtain a material composition with a minimum Pt-loading, which should maintain high electrocatalytic efficiency and reduce DEFC volume and weight [7]. Moreover, depending on the deposition method employed, the platinum utilization in membrane-electrode assemblies (MEA) of PEMFCs can be low. This is associated with the lack of electrolytic pathway between some catalyst particles and the PEM, which becomes electrochemically inactive. So high performance MEAs containing low Pt-loadings can be manufactured. There are several ways to produce such MEA: the thin-film method, electrodeposition, sputter, dual ion-beam assisted and electroless deposition [8–14]. Another way to produce electrocatalysts with high platinum utilization in MEA is to use pulse electrodeposition, once platinum is deposited only on ionic and electronic conducting pathways [7].

* Corresponding author. Tel.: +55 16 36024862; fax: +55 16 36332660.
E-mail address: fritz@ffclrp.usp.br (F. Huguenin).

0378-7753/$ – see front matter © 2008 Elsevier B.V. All rights reserved.
doi:10.1016/j.jpowsour.2008.07.024

Another approach for manufacturing MEAs with low-Pt-loadings and high platinum utilization is to employ the layer-by-layer (LbL) technique, which is based on physical adsorption of oppositely charged layers [15,16]. One specific advantage of this method is that the film can be self-assembled to the PEM surface without degradation, ensuring a high electrolytic connectivity between catalyst nanoparticles and ionic conductors [17]. Another advantage of the LbL method is the high control of the thickness and nanoarchitecture of the thin-films [18–20]. Manipulating polymers, metal oxides and metallic particles at the nanometer scale is also a viable means of optimizing electrocatalytic properties for alcohol electrooxidation [21,22].

Pt/SnO_2 and Pt/Sn catalysts have been thoroughly investigated, and they are considered promising anodes for ethanol electrooxidation [23–28]. According to the bifunctional mechanism shown below, SnO_2 or Sn can promote formation of oxygen-like species (Reaction (1)), because of the water dissociation reaction at low potentials. This favors the oxidative removal of CO-like species produced from cleavage of ethanol bonds (Reaction (2)) that are strongly adsorbed on adjacent Pt sites, thus liberating the latter (Reaction (3)) [23–29].

$$Pt + SnO_2 + 2H_2O \rightarrow Pt(OH) + SnO_2(OH) + 2H^+ + 2e^- \quad (1)$$

$$2Pt + CH_3CH_2OH \rightarrow Pt(CO) + Pt(res) + xH^+ + xe^- \quad (2)$$

$$Pt(CO), Pt(res) + Pt(OH) + SnO_2(OH) \rightarrow CO_2 + Pt + SnO_2 + xH^+ + xe^- \quad (3)$$

where Pt(OH), Pt(CO) and Pt(res) represent strongly adsorbed oxygen-like species, carbon monoxide and organic residues (other carbon-like species than carbon monoxide) on platinum sites, respectively. SnO_2(OH) represents adsorbed oxygen-like species on SnO_2. This general scheme is simplified and corresponds to the reaction via formation of CO_2 only.

The promoting effect can also be associated with the electronic properties, which also favor CO oxidation at low potentials, thus enhancing the electrocatalytic activity of the Pt/Sn catalyst compared with the Pt catalyst. Furthermore, other factors can be changed to increase catalytic activity. For instance, changing the substrate, preparation method and particle size can increase the availability of defect sites on the metal surface, which serve as nucleation center for the adsorption of oxygen-like species. Arenz et al. have investigated the catalytic activity of Pt nanoparticles ranging from 1 to 30 nm for CO electrooxidation, and they found an association between the oxophilicity of the nanoparticles and the number of defects [30].

In this work, Pt nanoparticles of several sizes were electrodeposited onto LbL films formed from SnO_2/polyallylamine (PAH), and their electrocatalytic activity in ethanol electrooxidation was investigated. SnO_2 was chosen as self-assembled matrix because this oxide enhances the electrocatalytic activity of Pt nanoparticles. Moreover, this oxide is stable in diluted acidic solution and serves as an electronic conductor pathway for Pt electrodeposition [31]. PAH was chosen because it easily produces self-assembled films with metal oxides, not to mention its high thermal stability, which is necessary for the thermal treatment carried out during SnO_2 preparation [32–34]. Specifically, the influence of the self-assembled matrices on the electrocatalytic properties of platinum nanoparticles for ethanol electrooxidation is investigated in this work.

2. Experimental

For preparation of the SnO_xH_y dispersion, a tin (IV) chloride solution in ethanol was added to an NH_4OH aqueous solution. The prepared suspensions were then refluxed for 3 h. The resulting powder was isolated by centrifugation and washed with water several times. It was then fully redispersed in water. Commercial PAH (with molecular weight of 56,000 g mol^{-1}) was purchased from Aldrich. The concentration of these dispersions was 1.6 g L^{-1}.

The LbL films formed from SnO_xH_y/PAH were assembled onto gold wire substrates, via ionic attraction of the oppositely charged materials. The substrate was immersed alternately for 1 min into the anionic (SnO_2, pH 8.2) and polycationic (PAH, pH 2.0) dispersions. After deposition of each layer, the substrates were rinsed in HCl solution (pH 2) for 30 s and dried under a nitrogen flow. 15-bilayer LBL films of SnO_2/PAH (with a geometrical area of 0.07 cm^2) were placed in an electrochemical cell containing a 0.1 mol L^{-1} H_2PtCl_6 (Aldrich) solution. The Pt–SnO_xH_y/PAH films were heated at 300 °C for 2 h, to produce Pt–SnO_2/PAH films, which presented greater chemical stability in acid medium. A current of 100 μA was applied for 1, 2, 5, and 10 min, leading to several Pt–SnO_2/PAH electrodes designated Pt1, Pt2, Pt5, and Pt10, respectively. After Pt electrodeposition, the electrodes were rinsed and dried as cited above. Platinum particles were also electrodeposited on 15-layer SnO_2 films prepared by the dip-coating technique, for comparison purposes. In the case of the dip-coating film, Pt was deposited under a current of 100 μA for 1 min, and this electrode was named Pt1dip. Pure platinum electrode (wire) was named Pt.

Scanning tunnel microscopy (STM) measurements were performed in a SPM multimode-Nanoscope III from Digital Instruments. High resolution transmission electron microscopy (HRTEM) images were obtained with a Philips CM200 equipment. X-ray diffraction measurements were carried out on a Siemens D5005 diffractometer using monochromatic Cu Kα radiation at 1.54 Å. The X-ray diffraction patterns obtained for the dip-coating and LbL films annealed at 300 °C and without thermal treatment can be assigned to the cassiterite SnO_2 structure. The average size of the nanoparticles was calculated on the basis of the Scherrer equation, as shown in the following equation

$$L = \frac{k\lambda}{\beta \cos \theta} \quad (4)$$

where k is the Scherrer shape factor (0.94), λ is the X-ray wavelength, β is the peak full width at half-maximum in radians, and θ is the diffraction peak position. The nanoparticle size for SnO_2 and SnO_xH_y was calculated by fitting the ⟨2 1 1⟩ diffraction peak of SnO_2, which was 4.7 nm for the casting and LbL films with and without thermal treatment.

In the electrochemical experiments carried out with an Autolab PGSTAT30 potentiostat/galvanostat, the counter electrode was a platinum sheet with an area of 8 cm^2, the reference electrode was the reversible hydrogen electrode (RHE), and the electrolytic solution was 0.5 mol L^{-1} H_2SO_4.

3. Results and discussion

Thin oxide nanocrystals can be identified by HRTEM image, shown in Fig. 1. These particles are practically spherical and have an effective mean diameter of 4.0 nm, with a narrow size distribution (ranging from 3 to 6 nm), without aggregates or cluster formation.

Fig. 2a–d shows the STM images for Pt1, Pt1dip, Pt2, and Pt10, respectively. The platinum particle distribution is similar for the Pt1 and Pt1dip electrodes. The diameter of sphere-like platinum particles is about 1.8 nm for both electrodes. Particles in the Pt2 and Pt10 electrodes are aggregated, and the size distribution is wider than that observed for the Pt1 electrode. The particle diameters range from 3 to 5 nm for the Pt2 electrode, and the mean diameter is 4 nm. In the case of the Pt10 electrode, the particle diameters range from 4 to 10 nm, and the mean diameter is about 7 nm. Although it

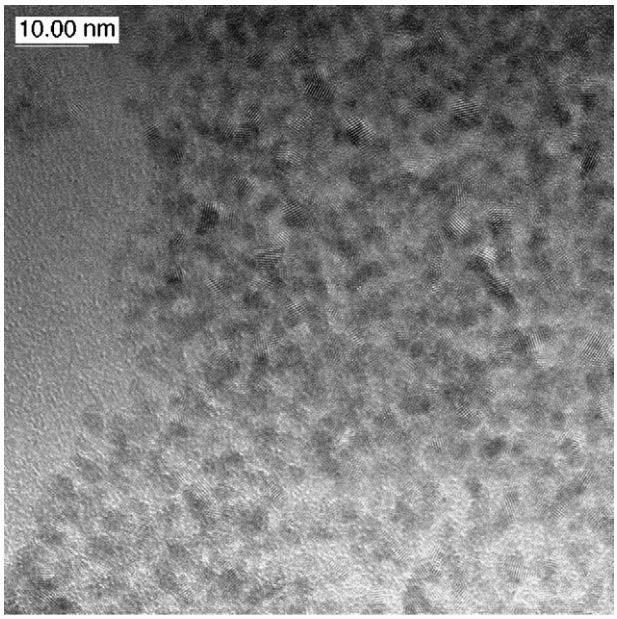

Fig. 1. HRTEM image of SnO_xH_y nanocrystals. Scale bar = 10 nm.

is not possible to distinguish between platinum and SnO_2 particles for the two latter electrodes, particle size increases as a function of the metallic platinum electrodeposition time, suggesting that the platinum size also increases from the Pt1 to the Pt10 electrode.

Fig. 3 shows the cyclic voltammograms of Pt1, Pt1dip, Pt2, and Pt10 in 0.5 mol L^{-1} H_2SO_4 with a sweeping rate of 50 mV s^{-1}. The current observed during the positive/negative potential scan between 0.05 and 0.35 V is associated with the desorption/adsorption of atomic hydrogen on the surface of the electrodeposited platinum particles. Based on the charge values associated with atomic hydrogen desorption, and considering that this charge corresponds to 210 μC for a platinum area of 1 cm^2 [35], the real area of exposed platinum for Pt1, Pt1dip, Pt2, and Pt10 was 45×10^{-3}, 29×10^{-3}, 52×10^{-3}, and 197×10^{-3} cm^2, respectively. The ratio between the real area and the electrodeposition charge (electroreduction charge from Pt^{4+} to Pt^0) is 7.5, 4.8, 4.3, and 3.3 cm^2 C^{-1} for Pt1, Pt1dip, Pt2, and Pt10, respectively. The relation between these values and the electrodeposition time depends on several features such as size, geometry, and the degree of SnO_2 and/or PAH coverage on the platinum sites, for instance. Certainly, particle size and aggregates formation are some of the possible explanations for the tendency observed in these area/charge ratios, as observed in the images shown in Fig. 2. This suggests that the particles and aggregates observed in STM images, which increase as a function of the electrodeposition time, are associated with deposited platinum.

A well-defined capacitive current at the potential region between 0.4 and 0.65 V during the positive potential scan for the

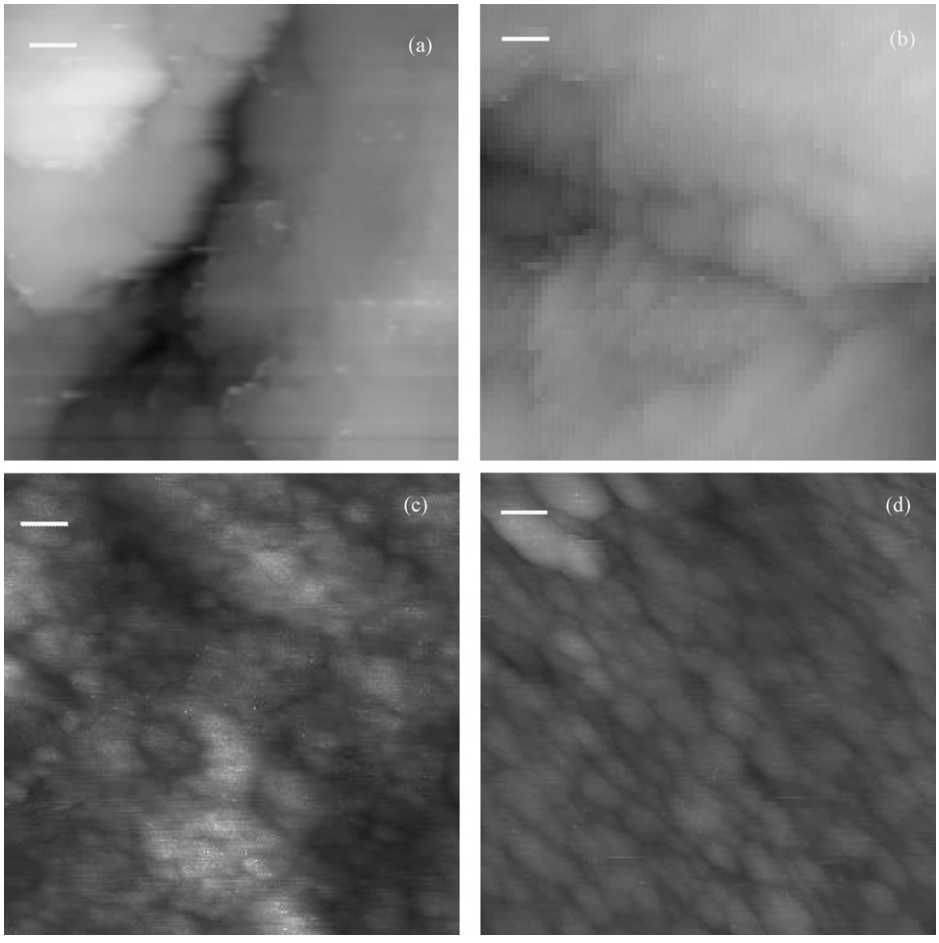

Fig. 2. STM images of (a) Pt1, (b) Pt1dip, (c) Pt2, and (d) Pt10 films. Scale bar = 10 nm.

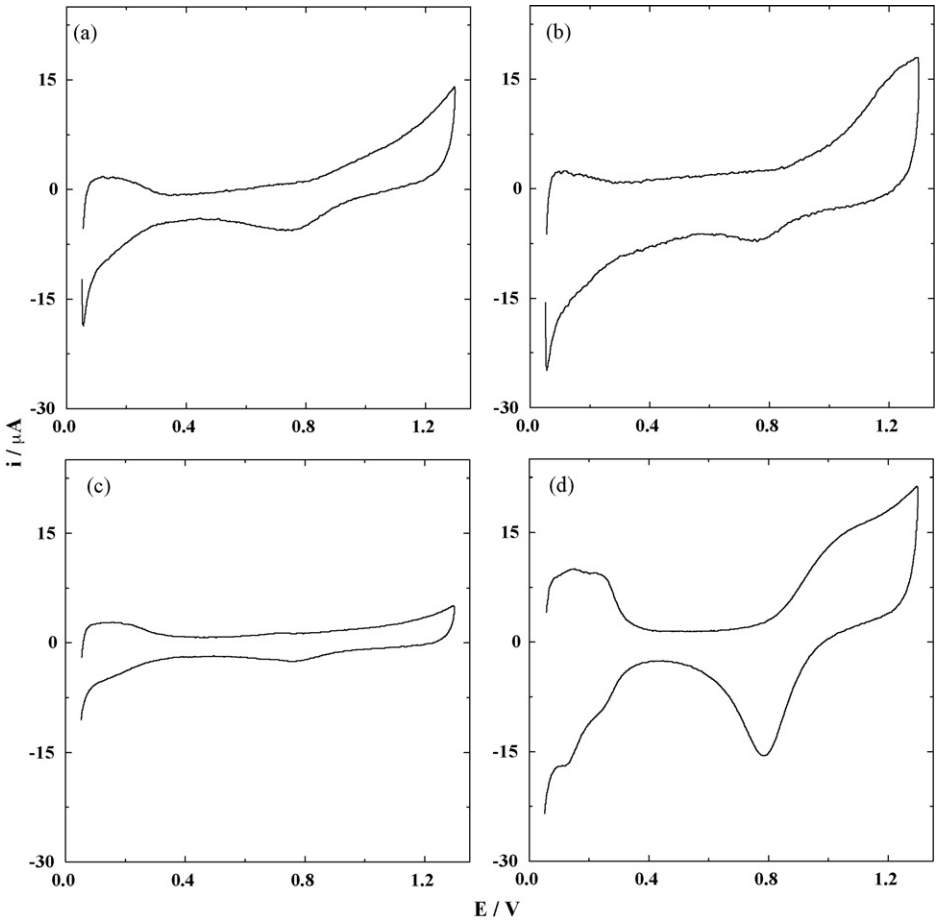

Fig. 3. Cyclic voltammograms for (a) Pt1, (b) Pt1dip, (c) Pt2, and (d) Pt10 in 0.5 mol L^{-1} H_2SO_4. $\nu = 50$ mV s^{-1}.

Pt10 electrode can also be noted. The Faradaic current associated with the formation of oxygen-like species adsorbed on the platinum particle surface (Reaction (1)) can be observed for potentials more positive than 0.65 V [24]. However, this reaction occurs at less positive potentials in the case of smaller particles. Contrary to the Pt10 electrode, the formation of adsorbed oxygen-like species begins at *ca*. 0.4 V for the Pt1 electrode. During the negative potential scan the reduction peak associated with the electroreduction of these oxygen-like species adsorbed on platinum sites is shifted toward more positive potentials as a function of the electrodeposition time. Specifically, this peak is shifted from 0.74 V for the Pt1 electrode to 0.79 V for the Pt10 electrode. These results suggest the presence of more oxophilic platinum nanoparticles in Pt1 compared with the other electrodes [30].

Electrochemical impedance spectroscopy measurements were accomplished for the electrodes at 0.7 V with 5 mV of superimposed *ac*. amplitude. Fig. 4 shows the Nyquist diagrams in 0.5 mol L^{-1} H_2SO_4 for: (a) Pt, (b) Pt10, (c) Pt1, and (d) Pt1dip. These diagrams display the semicircle or the beginning of a semicircle associated with the coupling of the charge transfer resistance of the water dissociation reaction, R_{ct}, and the interfacial capacitance, C_i, which is the sum of the double-layer capacitance and the adsorption pseudo-capacitance due to the adsorbed oxygen-like species. Aiming at only extrapolating the experimental data so as to determine the R_{ct} values, the fitting was done with a parallel $R_{ct}C_i$ circuit. Using the geometrical area of the electrodes, the R_{ct} values were 300, 170, 9, and 200 kΩ cm^2 for Pt, Pt10, Pt1 and Pt1dip, respectively, while the C_i values were 38.0, 11.0, 3.5, and 15.0 μF cm^{-2} for Pt, Pt10, Pt1, and Pt1dip, respectively. The R_{ct} values of the LbL electrodes increase as a function of the electrodeposition time. Using the real area of exposed platinum obtained from the cyclic voltammograms, the difference between these values is very significant: 315, 33.5, 0.4, and 5.8 kΩ cm^2 for Pt, Pt10, Pt1, and Pt1dip, respectively. So the amount of oxygen-like species adsorbed on the platinum particles must be higher for Pt1 than those of the other electrodes.

Fig. 5 shows the linear scan for Pt1, Pt1dip, Pt2, Pt5, Pt10 and Pt in 0.5 mol L^{-1} H_2SO_4 and 0.5 mol L^{-1} EtOH, at a sweeping rate of 10 mV s^{-1}. The current was normalized by the exposed platinum area for each of the electrodes. The potentiodynamic profiles of these curves are different, which indicates distinct reaction pathways. Based on the current density values between 0.2 and 0.8 V, the electrocatalytic activity increases as a function of particle size, according to the sequence: Pt10 > Pt5 > Pt2. The onset of ethanol oxidation is at *ca*. 0.45, 0.55, and 0.6 V for Pt10, Pt5, and Pt2, respectively. This suggests that the amount of non-covered adjacent platinum sites increases as a function of particle size, once a minimum number of adjacent platinum atoms is necessary for ethanol oxidative adsorption (Reaction (2)). In fact, the electrocatalytic activity of the Pt electrode for ethanol oxidation reaction is higher than that for the Pt–SnO_2/PAH electrodes, except for the Pt1 electrode. This enhancement in the catalytic activity of Pt1 can be associated to the large amount of oxygen-like species adsorbed on platinum atoms, as suggested from the cyclic voltammetry and impedance spectroscopy data, which removes the ethanol fragments (carbon monoxide and/or other carbon-like species) adsorbed on adjacent Pt atoms [26].

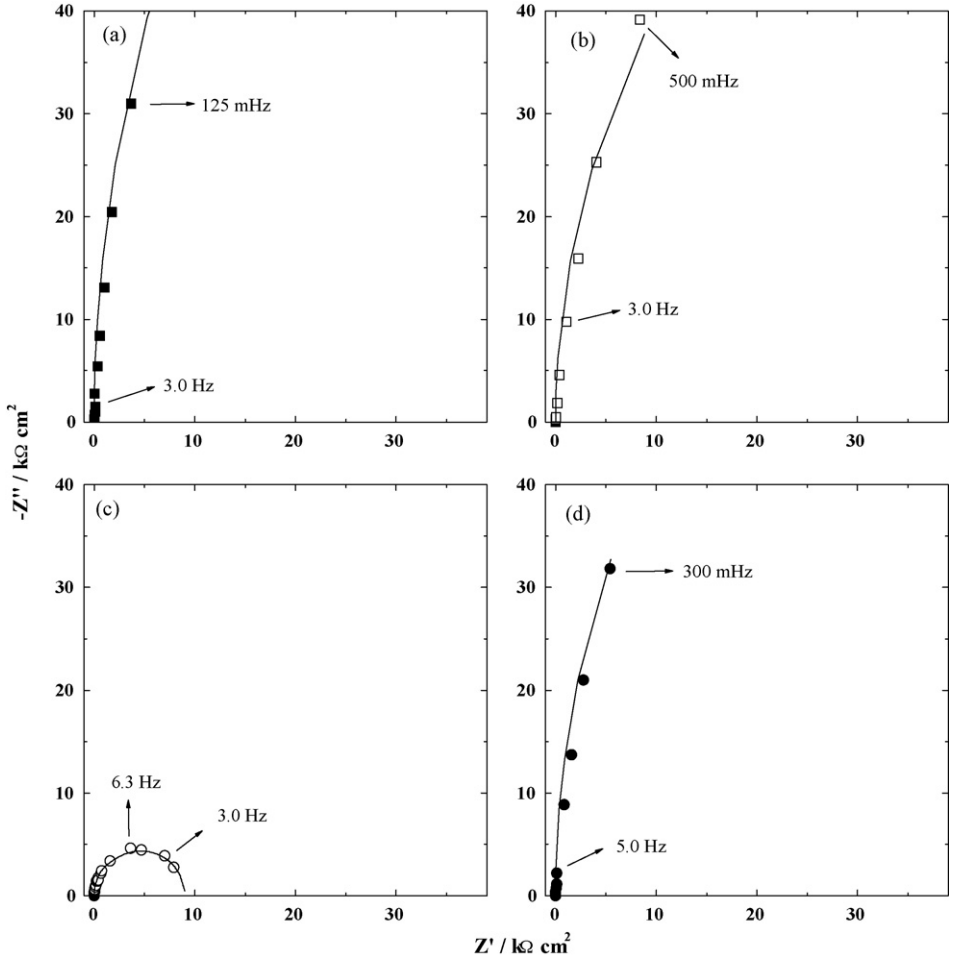

Fig. 4. Nyquist diagram for (a) Pt, (b) Pt10, (c) Pt1, and (d) Pt1dip in 0.5 mol L^{-1} H_2SO_4, E = 0.7 V. Solid lines correspond to the fitting data.

The electronic properties and/or the formation of oxygen-like species on SnO_2, which favors the bifunctional mechanism, can contribute for the electrocatalytic activity of the platinum nanoparticles for ethanol oxidation. However, other effects can also influence the electrocatalytic properties, once the electrocatalytic activity of Pt1dip for ethanol oxidation is lower than that of Pt1 and, in these electrodes, the platinum nanoparticles are sphere-like with similar size and distribution. A possibility could be that the presence of PAH and/or the self-assembled structure from SnO_2/PAH interfere in the nucleation step of the platinum nanoparticles, thus forming surface irregularities and serving as a nucleation center for OH adsorption [30]. However, more evidences are necessary to attribute the high electrocatalytic activity of the Pt1 electrode to these surface irregularities.

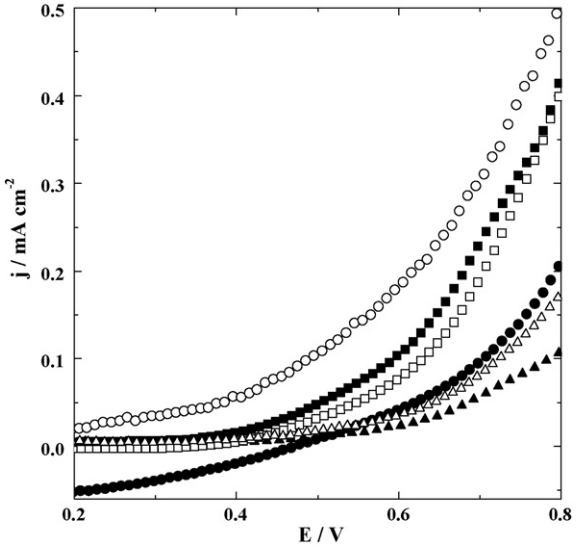

Fig. 5. Linear scan for (○) Pt1, (●) Pt1dip, (▲) Pt2, (△) Pt5, (□) Pt10, and (■) Pt in 0.5 mol L^{-1} H_2SO_4 and 0.5 mol L^{-1} EtOH. ν = 10 mV s^{-1}.

Fig. 6 shows the Nyquist diagrams for the electrodes in 0.5 mol L^{-1} H_2SO_4 and 0.5 mol L^{-1} ethanol at 0.7 V with 5 mV of superimposed *ac*. amplitude: (a) Pt and Pt1; (b) Pt10 and Pt1dip. The R_{ct} values associated with the ethanol electrooxidation were determined by fitting the experimental values with a parallel $R_{ct}C_i$ circuit. Using the geometrical area of the electrodes, the R_{ct} values were 4.3, 11.0, 70.0, and 140.0 kΩ cm^2 for Pt, Pt1, Pt10, and Pt1dip, respectively, while the C_i values were 20.0 μF cm^{-2} for Pt and Pt1, and 19 μF cm^{-2} for Pt10 and Pt1dip. Using the real area, the R_{ct} values associated with ethanol oxidation were 4.3, 0.5, 13.9, and 4.0 kΩ cm^2 for Pt, Pt1, Pt10 and Pt1dip, respectively. These values and the high relaxation frequency associated with the charge transfer and capacitive processes confirm the highest electrocatalytic activity of the Pt1 electrode. However, contrary to other electrodes, the R_{ct} value for Pt1 increases slightly in the presence of ethanol. Considering that Reactions (1) and (2) are parallel, and that the R_{ct} values for the Pt1 electrode in the absence and presence of ethanol

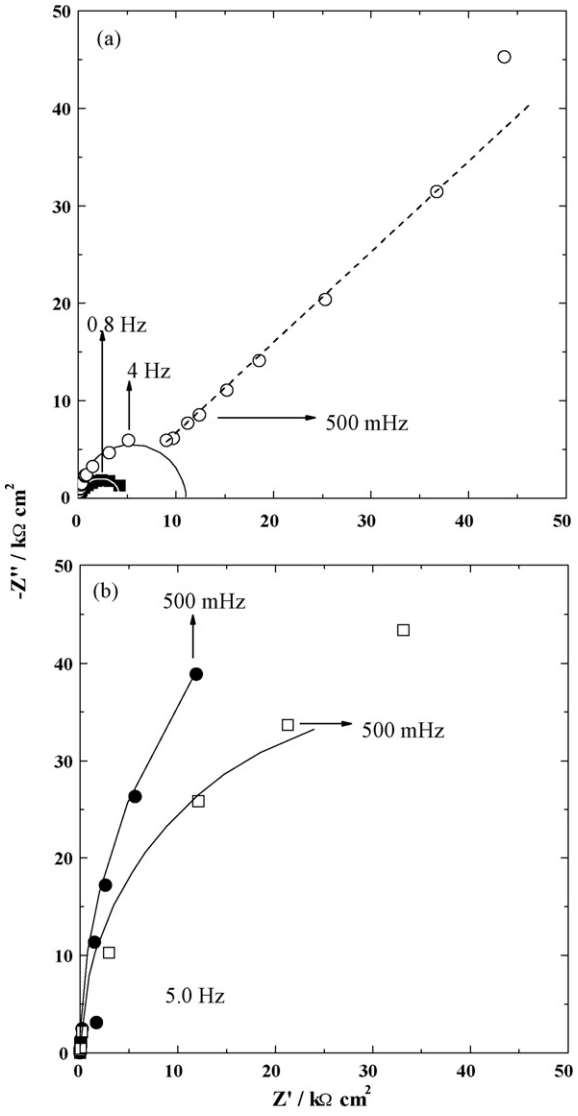

Fig. 6. Nyquist diagram for: (a) Pt (■) and Pt1 (○); (b) Pt10 (□) and Pt1dip (●) in 0.5 mol L^{-1} H_2SO_4 and 0.5 mol L^{-1} EtOH, E = 0.7 V.

are close, it is suggested that the formation of carbon-like species is slower than the formation of oxygen-like species due to the high oxophilicity of the platinum nanoparticles. We believe that the coverage of SnO_2/PAH on the neighboring platinum atoms is one of the reasons for the slow production of carbon-like species on the Pt1 electrode. The R_{ct} value for the Pt electrode in the presence of ethanol decreases significantly compared with the R_{ct} value in the absence of ethanol. In this case, the slowest step for Pt electrode is the formation of oxygen-like species. For the Pt10 and Pt1dip electrodes, there is also a decrease in R_{ct} values after addition of ethanol to the electrolytic solution. However, the change in these values is lower than that in the case of Pt electrode. This can be associated with the coverage of SnO_2 and/or PAH on the neighboring platinum atoms, as suggested above.

The Nyquist diagram of the Pt1 electrode is also a straight line at low frequencies. The slope is approximately 45° with the real axis, indicating a semi-infinite diffusion process into the LbL matrix. This process is not observed for other Pt–SnO_2/PAH electrodes because the charge transfer associated with ethanol electrooxidation is slower than that for the Pt1 electrode. Moreover, strong bonding between CO and small platinum particles decrease the CO diffusion rate, hindering its oxidation to CO_2 [36,37]. This transport mass effect can also be associated with the small amount of nanoparticles for Pt1 electrodes, which delays the diffusion of ethanol and/or some reaction intermediates. So if the amount of larger platinum nanoparticles is increased, with the same surface structure as that dispersed in the Pt1 electrode, the catalytic activity of the SnO_2/PAH electrodes for ethanol electrooxidation can be even more enhanced due to the smaller influence of the mass transport effects. Chemical methods are being tested for this proposal.

4. Conclusions

We have prepared platinum nanoparticles dispersed in self-assembled SnO_2/PAH films. Starting from a colloidal SnO_2 dispersion, LbL films of SnO_2/PAH were grown on gold substrate, and the metallic nanoparticles were electrodeposited at controlled current and time. Particle size and nanoparticle aggregation increase as a function of the electrodeposition time. Cyclic voltammetry and electrochemical impedance spectroscopy measurements have demonstrated that the smallest platinum particle (≈1.7 nm) displays high electrocatalytic activity for the water dissociation reaction. Oxygen-like species were formed on the platinum surface during the positive potential sweep for a less positive potential range as the particle size decreased. The oxophilicity of these nanoparticles as a function of the particle size was also evaluated by the shift of the voltammetric peak associated with the electroreduction of absorbed oxygenated species. Although the self-assembled matrix covers a fraction of neighboring electroactive sites necessary for the cleavage of ethanol bonds, the formation of oxygen-like species on these oxophilic centers in a less positive potential range ensured a high electrocatalytic activity for ethanol electrooxidation, according to the bifunctional mechanism. Therefore, platinum nanoparticles with controlled size and dispersed in these SnO_2/PAH matrices can be good candidates for use in the MEA of DEFCs.

Acknowledgements

C.B.B. and R.L.T.P. thank CNPq/PIBIC (no. 07.1.800.59.5) and FAPESP (no. 2006/06035-7) for the scholarships, respectively. We are grateful to FAPESP (05/00106-7), CNPq (555436/2006-3 and 550581/2005-7), and IMMP/MCT for financial support. We are also grateful to Professor Osvaldo Novaes Oliveira Jr. (IFSC/USP) and Dr. Marcelo Pereira da Silva (IFSC/USP) for the STM images.

References

[1] C. Stone, Fuel Cells Bull. 2007 (2007) 12.
[2] C. Lamy, J.-M. Léger, J. Phys. IV 4 (1994) C1.
[3] P.E. Tsiakaras, J. Power Sources 171 (2007) 107.
[4] S. Rousseau, C. Coutanceau, C. Lamy, J. Léger, J. Power Sources 158 (2006) 18.
[5] G. Camara, R. Lima, T. Iwasita, Electrochem. Commun. 6 (2004) 812.
[6] F. Colmati, E. Antolini, E. Gonzalez, Appl. Catal. B: Environ. 73 (2007) 106.
[7] J.-H. Wee, K.-Y. Lee, S.H. Kim, J. Power Sources 165 (2007) 667.
[8] M.S. Wilson, S. Gottesfeld, J. Electrochem. Soc. 139 (1992) L28.
[9] E.A. Ticianelli, C.R. Derouin, S. Srinivasan, J. Electroanal. Chem. 251 (1988) 275.
[10] A.T. Haug, R.E. White, J.W. Weidner, W. Huang, S. Shi, T. Stoner, N. Rana, J. Electrochem. Soc. 149 (2002) A280.
[11] A.D. Taylor, E.Y. Kim, V.P. Humes, J. Kizuka, L.T. Thompson, J. Power Sources 171 (2007) 101.
[12] G. Sasikumar, J.W. Ihm, H. Ryu, Electrochim. Acta 50 (2004) 601.
[13] C.K. Witham, W. Chun, T.I. Valdez, S.R. Narayanan, Electrochem. Solid-State Lett. 3 (2000) 497.
[14] S.Y. Cha, W.M. Lee, J. Electrochem. Soc. 146 (1999) 4055.
[15] F. Crespilho, F. Huguenin, V. Zucolotto, P. Olivi, F.C. Nart, O.N. Oliveira, Electrochem. Commun. 8 (2006) 348.
[16] L.C. Cogo, M.V. Batisti, M.A. Pereira-da-Silva, O.N. Oliveira, F.C. Nart, F. Huguenin, J. Power Sources 158 (2006) 160.
[17] M. Pan, H.L. Tang, S.P. Jiang, Z. Liu, Electrochem. Commun. 7 (2005) 119.

[18] J.L. Lutkenhaus, P. Hammond, Soft Mater. 3 (2007) 804.
[19] T.R. Farhat, P.T. Hammond, Adv. Funct. Mater. 16 (2006) 433.
[20] S.P. Jiang, Z. Liu, Z.Q. Tian, Adv. Mater. 18 (2006) 1068.
[21] A.A. Mikhaylova, E.B. Molodkina, O.A. Khazova, V.S. Bagotzky, J. Electroanal. Chem. 509 (2001) 119.
[22] L.P.R. Profeti, F.C. Simões, P. Olivi, K.B. Kokoh, C. Coutanceau, J.-M. Léger, C. Lamy, J. Power Sources 158 (2006) 1195.
[23] S.Q. Song, P. Tsiakaras, Appl. Catal. B 63 (2006) 187.
[24] F. Vigier, C. Coutanceau, F. Hahn, E.M. Belgsir, C. Lamy, J. Electroanal. Chem. 563 (2004) 81.
[25] G. Li, P.G. Pickup, J. Power Sources 173 (2007) 121.
[26] F.C. Simões, D.M. dos Anjos, F. Vigier, J.-M. Léger, F. Hahn, C. Coutanceau, E.R. Gonzalez, G. Tremiliosi-Filho, A.R. de Andrade, P. Olivi, K.B. Kokoh, J. Power Sources 167 (2007) 1.
[27] L. Jiang, G. Sun, Z. Zhou, S. Sun, Q. Wang, S. Yan, H. Li, J. Tian, J. Guo, B. Zhou, Q. Xin, J. Phys. Chem. B 109 (2005) 8774.
[28] L. Jiang, G. Sun, S. Sun, J. Liu, S. Tang, H. Li, B. Zhou, Q. Xin, Electrochim. Acta 50 (2005) 5384.
[29] X.H. Xia, H.-D. Liess, T. Iwasita, J. Electroanal. Chem. 437 (1997) 233.
[30] M. Arenz, K.J.J. Mayrhofer, V. Stamenkovic, B.B. Blizanac, T. Tomoyuki, P.N. Ross, N.M. Markovic, J. Am. Chem. Soc. 127 (2005) 6819.
[31] M.S. Saha, R. Li, X. Sun, Electrochem. Commun. 9 (2007) 2229.
[32] M. Ferreira, F. Huguenin, V. Zucolotto, J.E.P. da Silva, S.I.C. de Torresi, M.L.A. Temperini, R.M. Torresi, O.N. Oliveira, J. Phys. Chem. B 107 (2003) 8351.
[33] N.A. Galiote, F. Huguenin, J. Phys. Chem. C 111 (2007) 14911.
[34] S.J. Kim, S.J. Park, M.S. Shin, Y.H. Lee, N.G. Kim, S.I. Kim, J. Appl. Polym. Sci. 85 (2002) 1956.
[35] V.S. Bagotzky, Y.B. Vassilyev, Electrochim. Acta 12 (1967) 1323.
[36] K.A. Friedrich, F. Henglein, U. Stimming, W. Unkauf, Colloids Surf. A 134 (1998) 193.
[37] K.A. Friedrich, F. Henglein, U. Stimming, W. Unkauf, Electrochim. Acta 45 (2000) 3283.